ISBN 978-989-9121-53-9
43rd ISTANBUL International Conference on "Science, Technology, Humanities & Social Sciences" (STHSS-25)
Aug. 28-29, 2025 Istanbul (Turkiye)

LNAPL in Variational Hydraulic Gradients and its Impact on Soil Contamination

Harris Ramli[1], Kapil Kumar[1], Kong Chek Hung[1] and Mastura Azmi[1]

[1]School of Civil Engineering, Engineering Campus, Universiti Sains Malaysia, 14300, Nibong Tebal, Penang, Malaysia

***Abstract*:** *An investigation was conducted using two-dimensional experiments to evaluate the relationship between LNAPL spill volume, hydraulic gradient, and contamination behaviour. Using a Simplified Image Analysis Method (SIAM) to track diesel migration, the study found that spill volume and hydraulic gradient are the most critical factors influencing a contaminant plume's movement. A larger spill volume, with its greater mass, creates sufficient downward pressure to overcome capillary forces, causing deeper infiltration and bringing the pollutant closer to the groundwater. This significantly elevates the risk of groundwater contamination, especially in areas with fluctuating water tables. Conversely, the hydraulic gradient controls the plume's overall shape and spread. A high gradient leads to a dispersed, widespread plume with a lower concentration at the source, while a low gradient results in a more contained but highly concentrated plume near the spill point. These findings highlight that effective spill response requires an understanding of both the spill's volume and the site's hydraulic conditions. The study ultimately emphasises the importance of early detection and containment to prevent a localised soil contamination event from escalating into a widespread environmental disaster*

Keywords: *LNAPL Contamination, Groundwater Hydraulic Gradient, Capillary Fringe Depression, Contamination Plume, Lateral Migration*

1. Introduction

Groundwater remains one of the most dependable portable water sources for agriculture and daily use [1]–[2]. The coastal region is undergoing rapid industrial growth, driven by a favourable climate and plentiful water resources [3]. This industrial boom attracts more people seeking employment, increasing water consumption, and enhancing reliance on groundwater [4]. If this trend persists, water use is expected to continue rising. Therefore, contamination should be kept to a minimum or within permissible limits to prevent harm to the subsurface environment. Additionally, the coastal zone shows a dynamic atmosphere in the subsurface environment. This phenomenon occurs due to relatively high rainfall and wave action, which cause frequent fluctuations in groundwater levels [5]. Additionally, the water interface on the land creates a hydraulic gradient that serves as the driving force for pollutant movement. Moreover, the hydraulic gradient undergoes different phases, including periods of constant gradient, steepness changes, and gradient fluctuations, forming a slope pattern [6]. Handling subsurface contamination presents considerable challenges owing to the intricate characteristics of subsurface environments.

Hydrocarbon pollution is globally recognized for its durability and persistence, even under severe environmental conditions. It can be either soluble or insoluble in water. Insoluble pollutants, such as Non-Aqueous Phase Liquids (NAPLs), present additional complexity due to their varying densities and interactions with air and water within voids and present a significant environmental hazard [7]. Any liquids or organic compounds that are immiscible or do not dissolve in water are referred to as non-aqueous phase liquids (NAPLs).

NAPLs that do not mix or dissolve well in water are most frequently found in products that are processed from crude oil.

Based on their density in relation to water, NAPLs are divided into two categories: dense non-aqueous phase liquids (DNAPL) and light non-aqueous phase liquids (LNAPL). To put it simply, DNAPL is heavier than LNAPL, which is lighter than water. With water's density at a standard 1.0 g/cm³, LNAPLs are lighter, typically ranging from 0.6 to 0.9 g/cm³, while DNAPLs are heavier and can reach densities up to 1.7 g/cm³. The chemical compound and the composition of the LNAPL or DNAPL can affect the density of NAPLs.

They can pollute the environment through both natural processes and human activities, such as accidental oil spills at sea or leaks from underground pipelines and storage tanks. Over time, BTEX compounds, benzene, toluene, ethylbenzene, and xylene, can be released due to groundwater fluctuations, releasing toxic and carcinogenic substances. Additionally, it reduces permeability by filling voids that influence the soil and vegetation's oxygen cycle, thereby impacting vegetation, which plays a vital role at the shoreline by providing extra strength in the slope stability.

LANPL and DNAPL exhibit distinct migration behaviors during contamination. Based on density, LNAPL usually floats at the water table or encounters resistance from capillary fringes. In contrast, DNAPL, being denser than water, moves downward until it reaches an impermeable layer, after which it spreads horizontally [8]. Including porous media characteristics such as permeability, porosity, and particle size distribution, multiple driving forces such as gravity, advective flow, and gradient differences initiate the movement of LNAPL.

Spills of oil or LNAPL products always provide a serious risk because of the low density of LNAPL, which causes the pollutant to flow farther away from the release site. In addition to making cleaning and soil remediation more difficult, this condition increases the possibility of groundwater pollution. In alongside negatively impacting soil and groundwater, the contamination will release greenhouse gases that will persist for many years [9]. LNAPL products may consist of an intricate combination of several chemicals, similar to that of petrol and diesel, or they may consist of pure organic compounds.

Depending on their distinct water solubilities, the different LNAPL components may dissolve in the aqueous phase in trace amounts. Unfortunately, certain chemical substances in drinking water can be dangerous to people even at very low concentrations of a few parts per billion (ppb). Long-term contamination also results from the slow dissolving process caused by LNAPL's immiscible characteristics.

Accidents involving vessels carrying petroleum, pipeline ruptures, or storage tank malfunctions may cause unintentional spills into surface waters and groundwater in the oil industry. This is because millions of barrels of oil are extracted from the earth's surface annually, necessitating the management of an enormous quantity of oil. The contamination leakage will not be detected until a nearby drinking water well becomes contaminated, particularly if it occurs underground under these circumstances. Groundwater contamination by LNAPL, such as diesel, is known to increase environmental and health risks due to their toxicity and carcinogenic compounds such as benzene, toluene, ethylbenzene and xylene (BTEX) is often only discovered after a large-scale accident. The subsequent soil investigation required for such incidents is what reveals the hidden groundwater pollution [10]. This highlights how these significant events can be the only trigger for detecting a problem that has been developing unnoticed.

After an LNAPL release at the surface, it tends to migrate downward through the vadose zone. This movement is influenced by the LNAPL volume and the capillary fringe's height, which is affected by capillary pressure and may cause a depression in that zone [11]. Lateral migration occurs due to advective flow driven by the hydraulic gradient. The hydraulic gradient is the driving force behind groundwater flow. It represents the change in hydraulic head over a given distance. Groundwater flows from areas of higher hydraulic head to areas of lower hydraulic head, as illustrated in Fig. 1.

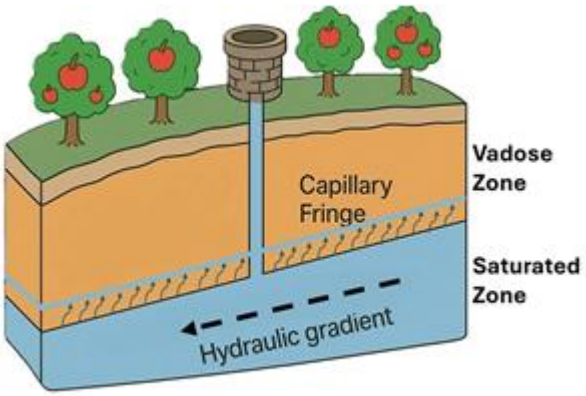

Fig. 1 Groundwater flow and hydraulic gradient.

In soil mechanics research, two primary types of hydraulic gradient are considered: the horizontal hydraulic gradient and the vertical hydraulic gradient. The horizontal hydraulic gradient pertains to the lateral spatial saturation that occurs under the influence of energy loss, specifically head loss. In simpler terms, it's like the slope of a hill for water. A steeper slope (a higher hydraulic gradient) means the water will flow faster, while a gentler slope (a lower hydraulic gradient) means it will flow more slowly.

Conversely, the vertical hydraulic gradient indicates whether water is attempting to flow vertically underground, influenced by differences in water levels at various depths [12]. The majority of aquifer flows, along with the inclination of the phreatic line due to hydraulic gradient, result in pollution dispersing laterally rather than vertically. The hydraulic gradient is defined as the interface where groundwater intersects with water bodies at the land-water interface. This indicates that any LNAPL that is released or leaked will migrate towards the nearest water bodies connected to the hydraulic gradient.

The shoreline, as well as coastal and riparian areas, are particularly susceptible to the contamination caused by LNAPL. This vulnerability arises from the dynamic interactions between surface and subsurface water in these landforms [13]–[14]. Furthermore, the stages of drainage and imbibition mimic the variability of the water table, which is influenced by seasonal tides, rainfall, and various anthropogenic activities. Such phenomena are particularly prevalent in coastal environments [15]. Based on the release source, LNAPL in soil can manifest in continuous and discrete forms. In cases of single-release events, the LNAPL is present in residual and entrapped forms. Entrapped and residual LNAPL continue to release as water tables fluctuate, driven by hydraulic gradients.

Soil remediation techniques have advanced since the 1970s, when the effects of LNAPL leaks on groundwater became a global concern. Over the past 50 years, the technique has developed in tandem with new technology, yet achieving remedial performance in a short amount of time remains challenging. There have been cases where diesel contamination has infiltrated municipal wells, even though the source of the contamination is not in the direction of groundwater flow, and cleanup from an industrial-scale spill accident would take more than ten years [16].

One of the main reasons for the complexity of the issue and the challenge of reaching the required residual LNAPL saturation target in remediation projects is the limited knowledge concerning the LNAPL migration behaviour. Thus, the main aim of this research is to investigate the capillary depression in the soil and the migration behaviour of LNAPL spills by diesel under variations of hydraulic gradient. This research aims to reveal how LNAPL spreads laterally in natural environments where groundwater is flowing. To accurately capture the complex movement of diesel and groundwater in the subsurface, we are using a Simplified Image Analysis Method (SIAM). This method is crucial for ensuring we collect all the necessary data from the experiment's dynamic conditions.

2. Simplified Image Analysis Method (SIAM) and Experimental Work

Many studies have explored LNAPL in subsurface environments using destructive and non-destructive methods, suited for in situ or ex-situ analysis. The choice depends on specific goals, problem characteristics, and resources. Our non-destructive image analysis approach is backed by prior research examining LNAPL fluctuations related to water table changes and volume variations through scale modeling.

Employing a methodology analogous to that utilized in image analysis, the distribution of LNAPL within a one-dimensional column model, under conditions of fluctuating water tables, was investigated by [17]. The findings revealed that LNAPL remains residual under the water table after the imbibition process. Similarly, a two-dimensional tank study in dual-porosity kaolin soil was carried out to assess the LNAPL at different rainfall intensities. The study revealed that entrapped LNAPL was present after the LNAPL fluctuated due to rainfall. This study explores a two-dimensional tank experiment conducted in dual-porosity kaolin soil, focusing on the behavior of LNAPL under varying rainfall intensities. The findings indicate that LNAPL became entrapped and persisted after fluctuations instigated by rainfall [18]. Based on previous research work, it is proven that the image analysis method is the best method to be used in investigating immiscible liquids such as LNAPL migration in the subsurface in complex dynamic natural groundwater conditions.

The SIAM is a method that measures the saturation distribution values for water and NAPL in granular soils across wide domains in real time [17]. In determining the temporal and spatial distribution of fluid saturations across the whole domain, this technique has been shown to be non-invasive and non-destructive. The Beer-Lambert Law of Transmissivity is used to compare the average optical densities of each matrix element with the average optical densities of the domains that are fully saturated with water (D_i^w), LNAPL (D_i^o), and completely dry (D_i^d), in order to get the saturation distribution matrices for water ([S_w]) and LNAPL ([S_o]).

To obtain the optical density data, two consumer-grade digital cameras with two different band-pass filters (*i* and *j*) were used. Equation (1) determines the average optical density (D_i) for the intensity of reflected light in a digital image. For a given spectral band *i*, d_{ji} stands for the optical density of individual pixels, indicates the intensity of the reflected light as determined by the values of individual pixels, I_{ji}^r, and I_{ji}^o indicates the intensity of light reflected by an ideal white surface [19]. *N* is the number of pixels in the area of interest. A matrix of correlations can be created using Equation (2) to determine the average optical density values for each mesh element in the domain under study.

$$D_i = \frac{1}{N}\sum_{j=i}^{N} d_{ji} = \frac{1}{N}\sum_{j=i}^{N}\left[-\log_{10}\left(\frac{I_{ji}^r}{I_{ji}^o}\right)\right] \tag{1}$$

$$\begin{bmatrix} D_i \\ D_j \end{bmatrix}_{mn} = \begin{bmatrix} (D_i^w - D_i^d)S_w + (D_i^o - D_i^d)S_o + D_i^d \\ (D_j^w - D_j^d)S_w + (D_j^o - D_j^d)S_o + D_j^d \end{bmatrix}_{mn} \tag{2}$$

The calibration procedure requires three calibrating photos (D_i^w, D_i^o, and D_i^d). The three calibration images represent the boundaries of the relationship plane and include the following: dry sand (S_w = 0%, S_o = 0%), sand completely saturated with LNAPL (S_w = 0%, S_o = 100%), and sand completely saturated with water (S_w = 100%, S_o = 0%). The values of [S_w] and [S_o] represent water saturation and NAPL saturation, respectively, as illustrated in Fig. 2.

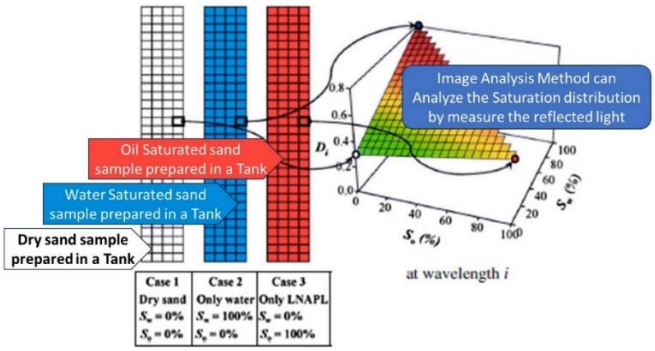

Fig. 2 Concept of SIAM (modified after [20])

Red Sudan III dye was applied to diesel to enhance its light-absorbing capabilities while Brilliant Blue FCF dye was applied to water to improve visibility. Diesel and water did not exhibit any noticeable modifications in their physical characteristics when both colours were applied at concentrations of 1:10,000 by weight. The soil particles neither absorb nor filter the dyes.

A 700 mm x 550 mm x 35 mm tank with transparent acrylic sides was used to investigate the two-dimensional lateral migration of diesel in porous media (sand). The tank was configured as shown in Fig. 3. The experiment took place in a darkened room using LED floodlights as a controlled lighting source. DSLR cameras with bandpass filters geared at 450 and 656 nm were used to take pictures. Photographs were taken at 5-minute intervals in the first hour and 15-minute intervals during the course of the experiment.

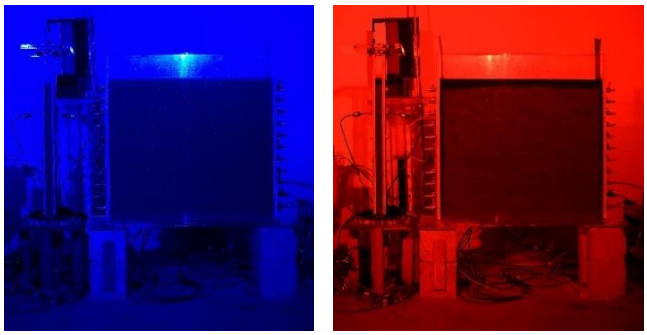

Fig. 3 Fully saturated tank setup before experiment start.

Each image was converted from NEF (Nikon proprietary RAW version files) to TIFF (Tagged Image File Format) using Nikon ViewNX 2.10.3. A MATLAB R2022b execution code that was developed in-house was used to analyse the TIFF pictures. With 450 nm and 656 nm bandpass filters, both images were examined in MATLAB R2022b. The diesel and water levels of saturation were then imported into an Excel worksheet for further investigation. Water circulation was set up to imitate the groundwater table and ensure unidirectional groundwater flow in order to evaluate diesel migration with respect to groundwater flow.

To investigate the dynamics of soil contamination, a comprehensive experimental design was implemented, as shown in Table 1, systematically varying both LNAPL spill volume and hydraulic gradient. The chosen parameters were intended to simulate a range of contamination scenarios, from minor spills to more severe events, and to understand their behaviour under different subsurface flow conditions.

The first stage of experiments, comprising M 2.4, L 2.4, M 0.7, and L 0.7, provided a foundational comparison. By testing two distinct hydraulic gradients, a high gradient of 2.413 and a low gradient of 0.714. These experiments also utilized two different spill volumes, enabling a direct assessment of how the quantity of contaminant influences its spread under both high and low flow regimes.

The second stage of the study was initiated with experiments H-S and M-S. These were designed to further investigate the critical 0.7 hydraulic gradient by introducing a new variable: a 35° slope on the top surface. The

hydraulic gradient of 0.700 is directly derived from the tangent of this 35° angle, linking the physical geometry of the setup to the hydrodynamic conditions. By conducting these experiments with a higher spill volume (400 mL) and a moderate volume (250 mL), the study aimed to understand the combined effects of a critical low-flow environment and a topographical feature on LNAPL plume dynamics.

TABLE I Volume of oil spill and hydraulic gradient for each experiment

Experiment	Oil Spill Volume (ml)	Surface (Spill Point)	Hydraulic Gradient, *i*
M 2.4	250	Flat	2.413
L 2.4	125	Flat	2.413
M 0.7	250	Flat	0.714
L 0.7	125	Flat	0.714
H-S	400	Slope 35°	0.700
M-S	250	Slope 35°	0.700

3. Behaviour of LNAPL in Variational Hydraulic Gradients

The first stage of the experiment began with the fully saturated sand being allowed to drain by gravity. Because of the great permeability of the sand, the water drained rather quickly, allowing for the observation of stable capillary fringe height in less than six hours. After spilling from the top of the tank, the diesel moved downward due to capillarity and gravity.

The quantity of spilt diesel was found to be a critical factor in its initial migration. When the 250 mL spill was introduced, it quickly overcame the soil's resistance and migrated rapidly towards the capillary fringe layer. This behaviour was distinctly different from the smaller 125 mL spill, which exhibited a less aggressive vertical descent. The final distribution patterns, shown in Fig. 4 for the 250 mL spill (M 2.4) and Fig. 5 for the 125 mL spill (L 2.4), visually confirm this difference. The greater mass and pressure head of the larger volume led to a more substantial infiltration, resulting in a significantly larger quantity of diesel accumulating in the capillary fringe at the conclusion of the experiment.

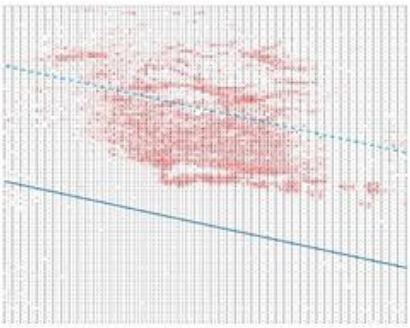

Fig. 4 Distribution of diesel in the tank at the end of Experiment M 2.4.

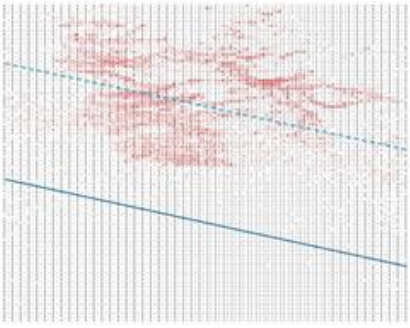

Fig. 5 Distribution of diesel in the tank at the end of Experiment L 2.4.

When an LNAPL, such as diesel, spills into the ground, its volume directly determines the severity of the contamination. A larger spill, with its greater downward pressure, can more effectively overcome the soil's natural resistance and capillary forces, pushing the pollutant deeper into the ground. This deeper infiltration places the contaminant perilously close to the groundwater layer, significantly increasing the risk of widespread contamination.

As natural groundwater levels fluctuate due to rainfall and seasonal changes, the rising water table will inevitably encounter the contaminated layer. This contact allows pollutants to be absorbed into the groundwater, transforming a localised soil spill into a major threat to our drinking water and ecosystems. In regions with frequent rainfall, this risk is amplified, as the constant rise and fall of the water table repeatedly exposes the groundwater to contaminants, accelerating their spread.

These experiments revealed that a larger spill volume, like the 250 mL diesel release, has sufficient pressure to breach the natural defence of the soil's fine pores, which are filled with water by capillary action. This means the contaminant is closer to the groundwater in the saturated zone. While both the 125 mL and 250 mL spills reached this layer, the larger volume exerted enough force to significantly cause capillary depression of its original height, demonstrating its greater potential for vertical migration. Similar results were also found by [21] when larger spill volumes, having more mass, are subject to a stronger gravitational pull, which causes a more significant depression of the capillary fringes.

Based on the first phase of the experiment, diesel will be significantly closer to the saturation zone in experiment M 0.7 due to the larger capillary depressions, where the hydraulic gradient is low and the diesel spill is high. Compared to any other experiment, the level of contamination at the precise spill source would be higher. A key finding of this study is the inverse relationship between the hydraulic gradient and the concentration of contamination at the spill source. Under conditions of a high hydraulic gradient, the strong horizontal groundwater flow acts as a powerful transport mechanism, which causes the contaminant to spread more broadly but with less concentration directly at the spill point. In contrast, a low hydraulic gradient leads to a more concentrated, but less extensive, contamination zone near the source.

This finding draws attention to the second stage of the study, in which only the low hydraulic gradient of 0.7 is considered. As in this step, the top of the soil is cut to a 35° slope, which is similar to the low hydraulic gradient of the previous stage. The lateral migration of LNAPL plumes was observed and quantitatively recorded, demonstrating different behaviour influenced by injection volume over time. The experimental data revealed a complex two-stage migration pattern for both the 250 mL spill (M-S) and 400 mL spill (H-S) of LNAPL volumes.

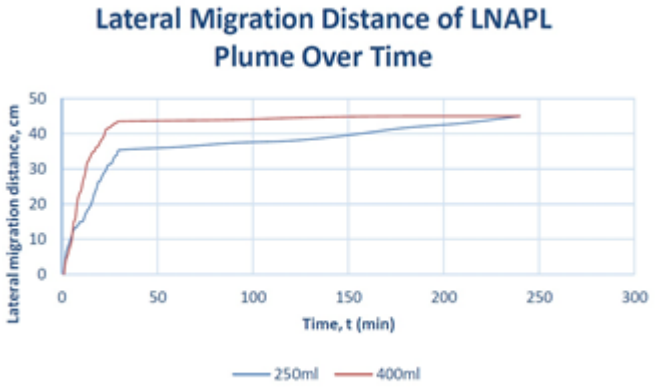

Fig. 6 Lateral diesel migration of H-S (400ml) and L-S (250ml).

During the initial period, the 250 mL injection exhibited a greater lateral migration distance than the 400 mL volume. This initial disparity is attributed to the greater gravitational force associated with the larger 400 mL volume, which promoted a more significant vertical infiltration into the saturated zone as shown in Fig. 6. In

contrast, the smaller mass of the 250 mL LNAPL resulted in a more immediate and balanced distribution across the horizontal plane, initiating lateral migration earlier. Subsequently, the migration dynamics shifted. The 400 mL plume accelerated its horizontal spread, surpassing the 250 mL plume. This change in behaviour is explained by the increased pressure head and saturation at the injection point of the larger volume, which generated a stronger driving gradient for lateral migration. The high permeability of the sand facilitated this rapid advancement, allowing the fluid to move freely through the pore spaces.

After the 30-minute mark, the rate of lateral migration for both plumes began to decline. This deceleration is attributed to the increasing saturation of the pore spaces, which heightened the resistance to further horizontal movement. The plumes continued to advance, albeit at a reduced velocity, until reaching the 45 cm boundary of the tank. The data confirm that the 400 mL plume reached the 45 cm boundary significantly earlier than the 250 mL plume, underscoring the direct effect of injection volume on plume reach and temporal dynamics.

These findings highlight the critical role of injection volume in determining the initial behavior, momentum, and overall extent of LNAPL migration. A higher volume not only leads to a faster plume expansion after the initial phase but also poses a greater contamination risk due to its ability to saturate a larger subsurface area more quickly. These results emphasize the importance of early monitoring and containment strategies for high-volume LNAPL spills, particularly in environments with high-permeability soils and dynamic groundwater conditions.

4. Conclusion

This study is being carried out to investigate the soil capillary depression due to LNAPL and the migration behaviour of LNAPL spills under various hydraulic gradients ranging from 0.700 to 3.571. Due to the experiment's dynamic condition, which included diesel migration and groundwater flow under hydraulic gradient, a Simplified Image Analysis Method (SIAM) was used. Based on the study, the volume of a spill and the hydraulic gradient are the two most critical factors determining the behaviour of a contaminant plume. A larger spill volume increases downward pressure, allowing the pollutant to more effectively breach the soil's defences and migrate deeper, closer to the groundwater. This poses a significant risk, particularly in areas where fluctuating groundwater levels can bring the water table into direct contact with the contaminated zone. Conversely, the hydraulic gradient dictates the plume's overall shape and spread. A high gradient causes the contaminant to disperse over a wide area, reducing the concentration at the source, while a low gradient results in a more contained but highly concentrated plume. This dual-factor analysis highlights that every spill is a unique challenge that requires tailored strategies. The study ultimately emphasises the importance of early detection and containment to prevent a localised soil contamination event from escalating into a widespread environmental disaster.

5. Acknowledgement

The authors wish to express sincere appreciation for the support from Universiti Sains Malaysia in making this project a success.

6. References

[1] Fitts, C. R. (2024). Groundwater contamination. In *Groundwater Science* (pp. 497–580). Elsevier. https://doi.org/10.1016/B978-0-12-811455-1.00017-4

[2] Narimani, R., Murgulet, I., & Murgulet, D. (2025). *Emerging Contaminants in Groundwater: Challenges, Management, and Policy Perspectives* (pp. 189–226). https://doi.org/10.1007/978-3-031-71758-1_9

[3] Han, D., & Currell, M. J. (2022). Review of drivers and threats to coastal groundwater quality in China. *Science of The Total Environment*, *806*, 150913. https://doi.org/10.1016/j.scitotenv.2021.150913

[4] Kumar, K., & Ramli, H. (2024). Improving coastal reservoir management through an update framework: Addressing the challenges of hydrocarbon spills and bluff stability. *Ocean & Coastal Management*, *256*, 107306. https://doi.org/10.1016/j.ocecoaman.2024.107306

[5] Al-Mannai, A. A. M., Ouerghi, S., & Elhag, M. (2025). Assessment of Coastal Zone Vulnerability in Context of Sea-Level Rise and Inundation Risk in Qatar. *Atmosphere*, *16*(5), 622. https://doi.org/10.3390/atmos16050622

[6] de Freitas, M. H., & Tellam, J. (2025). Chapter 2 Engineering geological principles of groundwater. *Geological Society, London, Engineering Geology Special Publications*, *31*(1). https://doi.org/10.1144/egsp31-2025-4
[7] Alden, D. F., García-Rincón, J., Rivett, M. O., Wealthall, G. P., & Thomson, N. R. (2024). *Complexities of Petroleum Hydrocarbon Contaminated Sites* (pp. 1–19). https://doi.org/10.1007/978-3-031-34447-3_1
[8] Redman, J. D. (2009). Contaminant Mapping. In *Ground Penetrating Radar Theory and Applications* (pp. 247–269). Elsevier. https://doi.org/10.1016/B978-0-444-53348-7.00008-9
[9] Sookhak Lari, K., Davis, G. B., Bastow, T., & Rayner, J. L. (2024). On quantifying global carbon emission from oil contaminated lands over centuries. *Science of the Total Environment*. 907. Available: https://doi.org/10.1016/j.scitotenv.2023.168039
[10] Liu, Y., Zhao, X., Wang, X., Ding, A., & Zhang, D. (2024). Application of whole-cell bioreporters for ecological risk assessment and bioremediation potential evaluation after a benzene exceedance accident in groundwater in Lanzhou, China. *Science of the Total Environment*. 906. Available: https://doi.org/10.1016/j.scitotenv.2023.168039
[11] Newell, C. J., Acree, S. D., Ross, R. R., & Huling, S. G. (1995). *Ground water issue: Light nonaqueous phase liquids*. Groundwater Services, Inc., Houston, TX (United States).
[12] Conlon, T. D., Wozniak, K. C., Woodcock, D., Herrera, N. B., Fisher, B. J., Morgan, D. S., Lee, K. K., & Hinkle, S. R. (2005). *Ground-water hydrology of the Willamette Basin, Oregon*. U. S. Geological Survey. https://doi.org/10.3133/sir20055168
[13] Afif Altaf Mohd Ezuan'Izam, Muhammad Affendi Alias, Nur Farisha Mohd Fakarruddin, & Suhaila Sahat. (2025). Coastal Erosion Hazard Map at Pantai Perpat and Pantai Punggur, Batu Pahat, Johor. *Multidisciplinary Applied Research And Innovation*, *6*(2), 119–126.
[14] Yadav, B. K., & Hassanizadeh, S. M. (2011). An overview of biodegradation of LNAPLs in coastal (Semi)-arid environment. In *Water, Air, and Soil Pollution* (Vol. 220, Issues 1–4, pp. 225–239). https://doi.org/10.1007/s11270-011-0749-1
https://doi.org/10.1007/s11270-011-0749-1
[15] Zhang, W., Yang, J., Yang, L., & Niyogi, D. (2022). Impacts of City Shape on Rainfall in Inland and Coastal Environments. *Earth's Future*, *10*(5). https://doi.org/10.1029/2022EF002654
[16] Ahad, J. M. E., Martel, R., & Calderhead, A. I. (2023). Isotope forensics of polycyclic aromatic compounds (PACs) in a contaminated shallow aquifer. *Chemosphere*. 140169. Available: https://doi.org/10.1016/j.chemosphere.2023.140169
[17] Flores, G., Katsumi, T., Inui, T., & Kamon, M. (2011). A simplified image analysis method to study lnapl migration in porous media. *Soils and Foundations*, *51*(5), 835–847. https://doi.org/10.3208/sandf.51.835
[18] Alazaiza, M. Y. D., Copty, N. K., & Abunada, Z. (2020). Experimental investigation of cosolvent flushing of DNAPL in double-porosity soil using light transmission visualization. *Journal of Hydrology*, *584*, 124659. https://doi.org/10.1016/j.jhydrol.2020.124659
[19] Kechavarzi, C., Soga, K., & Wiart, P. (2000). Multispectral image analysis method to determine dynamic fluid saturation distribution in two-dimensional three-fluid phase flow laboratory experiments. *Journal of Contaminant Hydrology*, *46(3–4), pp. 265–293.*
https://doi.org/10.1016/S0169-7722(00)00133-9
[20] Yimsiri, S., Euaapiwatch, S., Flores, G., Katsumi, T., & Likitlersuang, S. (2018). Effects of water table fluctuation on diesel fuel migration in one-dimensional laboratory study. *European Journal of Environmental and Civil Engineering, 22(3), pp. 359–385.*
https://doi.org/10.1080/19648189.2016.1197158
[21] Alazaiza, M. Y. D., Ramli, M. H., Copty, N. K., & Ling, M. C. (2021). Assessing the impact of water infiltration on LNAPL mobilization in sand column using simplified image analysis method. *Journal of Contaminant Hydrology*, *238*, 103769. https://doi.org/10.1016/j.jconhyd.2021.103769